Polymer 51 (2010) 2368–2375

Contents lists available at ScienceDirect

Polymer

journal homepage: www.elsevier.com/locate/polymer

The influence of carbon nanotube aspect ratio on the foam morphology of MWNT/PMMA nanocomposite foams

Limeng Chen, Rahmi Ozisik, Linda S. Schadler*

Department of Materials Science and Engineering, and Rensselaer Nanotechnology Center, Rensselaer Polytechnic Institute, Troy, NY 12180, USA

ARTICLE INFO

Article history:
Received 8 February 2010
Received in revised form
15 March 2010
Accepted 25 March 2010
Available online 31 March 2010

Keywords:
Polymer nanocomposite foams
Carbon nanotube
Aspect ratio

ABSTRACT

Polymer nanocomposite foams, products from the foaming of polymer nanocomposites, have received increasing attention in both the scientific and industrial communities. Nanocomposite foams filled with carbon nanofibers or carbon nanotubes with high electrical conductivity, enhanced mechanical properties, and low density are potential effective electromagnetic interference (EMI) shielding materials. The EMI shielding efficiency depends on the electrical conductivity and bubble density, which in turn, depend on the properties of the filler. In the current study, multi walled carbon nanotubes (MWNT) with controlled aspect ratio were used to alter the bubble density in MWNT/poly(methyl methacrylate) (PMMA) nanocomposites. It was found that the nanocomposite foams filled with shorter MWNT had higher bubble density under the same foaming conditions and MWNT concentration. Both the ends and sidewalls of carbon nanotubes can act as heterogeneous bubble nucleation sites, but the ends are more effective compared to the sidewalls. Shorter nanotubes provide more ends at constant MWNT concentration compared to long nanotubes. As a result, the difference in the foam morphology, particularly the bubble density, is due to the difference in the number of effective bubble nucleation sites.

1. Introduction

Electromagnetic interference (EMI) is undesirable because it disturbs the normal functioning of electronic appliances and may cause irradiative damage to the human body [1]. Conventional EMI shielding materials are common metals and their composites, which have high shielding effectiveness due to their high conductivity and high dielectric constant. While metals have good EMI shielding properties, they are heavy, and have poor corrosion resistance. Due to the desire for lightweight EMI shielding materials, conducting polymers and polymer based conducting composites have received much attention [2].

According to Schelkunoff [3], the EMI shielding effectiveness is the result of reflection loss, transmission or absorption loss, and reflection losses at internal interfaces. The shielding effectiveness is closely related to conductivity of the materials. The reflection loss is a function of the ratio σ_r/μ_r, and the absorption loss is a function of $\sigma_r\mu_r$, where σ_r is the electrical conductivity relative to copper and μ_r is the relative magnetic permeability [4]. Yuen and colleagues found that multi walled carbon nanotube/poly(methyl methacrylate) (MWNT/PMMA) composites prepared by in situ polymerization possessed higher shielding effectiveness than composites prepared by melt mixing. It was proposed that the adhesion between MWNT and PMMA in the former was better than in the latter, therefore the interface resistance was lower in the nanocomposites prepared by in situ polymerization. Lower interface resistance led to higher conductivity and thus, higher shielding effectiveness [2]. Li et al. increased the shielding effectiveness of MWNT/polyacrylate nanocomposite films by increasing the loading of MWNT, which increased the conductivity of the composite film [1].

In order to increase the shielding effectiveness through multiple internal reflections, conductive polymer nanocomposite foams have been developed [5] (see Fig. 1). The advantage of internal reflections is that the material absorbs and attenuates instead of reflecting electromagnetic radiation [6], which reduces damage to internal electronic circuits caused by reflected radiation. Yang et al. developed carbon nanofiber and carbon nanotube filled polystyrene conductive foams for lightweight EMI shielding [2]. They obtained a composite with a density of approximately 0.56 g/cm^3 and achieved an EMI shielding effectiveness of approximately 20 dB. Compared to carbon nanofiber filled composite foams, carbon nanotube filled foams had higher EMI shielding effectiveness at lower concentrations [2]. Thomassin et al. developed MWNT/polycaprolactone composite foams by

* Corresponding author. Tel.: +1 518 276 2022.
E-mail address: schadl@rpi.edu (L.S. Schadler).

0032-3861/$ – see front matter © 2010 Elsevier Ltd. All rights reserved.
doi:10.1016/j.polymer.2010.03.042

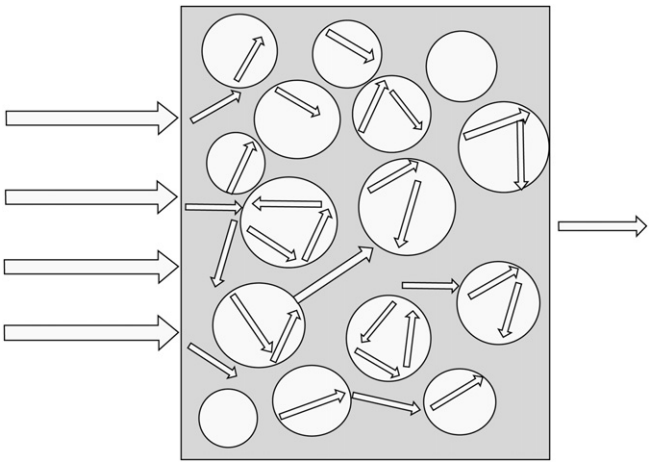

Fig. 1. Multiple reflections of electromagnetic waves in nanocomposite foams.

using supercritical CO_2 foaming technology and obtained EMI shielding effectiveness as high as 60–80 dB together with low reflectivity at very low volume concentrations of MWNT (0.25 vol %). The shielding effectiveness that Thomassin et al. achieved is comparable to that of the most efficient metallic EMI shielding materials [6]. They also found that increasing the carbon nanotube concentration can increase the shielding effectiveness, possibly due to increased conductivity [7].

Because the shielding effectiveness in conductive carbon nanotube/polymer composite foams results mostly from the loss due to internal multiple reflections, increasing the bubble density (and hence increasing internal area) should increase the shielding effectiveness [7]. However, there is a trade off. As the bubble density increases, the alignment of the nanotubes changes, which can decrease the conductivity and thus, the shielding effectiveness [7,8]. Controlling the properties of the MWNTs and the bubble density inside the nanocomposite foams to get high shielding effectiveness is of great importance for such EMI shielding applications.

The influence of carbon nanotube properties such as aspect ratio and surface chemistry on the properties of solid polymer nanocomposites have been extensively studied [8,9]. However, carbon nanotube/polymer composite foams are more complex than solid composites. The interactions between fillers, bubbles and matrix and their influence on the properties of composite foams are still not fully understood. In addition, the properties of one component may affect the properties of the other two. To produce polymer nanocomposite foams with desirable properties such as high electromagnetic wave shielding effectiveness or high strength, a better understanding of the interactions between fillers, bubbles and matrix is necessary. The influence of nanocomposite processing methods on the foam morphology of nanocomposite foams [10,11] has been reported, but the aspect ratio of the nanotube or nanofiber fillers may have changed due to the changes in processing and was not recorded. The filler aspect ratio likely alters the foam morphology. The current study is aimed at revealing the influence of MWNT aspect ratio on the bubble density of nanocomposite foams.

In the current study, MWNT/PMMA composites of controlled MWNT aspect ratio were foamed with supercritical CO_2 at various conditions. Supercritical CO_2 was chosen as the physical foaming agent due to its relatively low critical temperature (31 °C), low critical pressure (7.38 MPa) and non-toxic nature. The aspect ratio of the nanotubes was changed with the intent of understanding bubble nucleation in MWNT/PMMA nanocomposites.

2. Experimental

2.1. Materials

MWNTs were synthesized at Rensselaer using a chemical vapor deposition method on silicon wafers, details can be found in reference [12]. MWNTs with different lengths but similar diameters (~30 nm) were obtained by controlling the growth time. The growth rate was found to be approximately 1 μm per minute. Thermogravimetric analysis (TGA) of MWNTs indicated that there was less than 4.3% (by weight) catalyst in the sample.

Poly(methyl methacrylate), PMMA, was chosen as the composite matrix polymer because of its outstanding chemico-physical properties [13] and relatively high affinity for CO_2. Commercial grade PMMA (Plexiglas V920-100) was kindly donated by Altuglas International. Tetrohydrofuran (THF) and concentrated nitric acid were purchased from Sigma–Aldrich, and ethyl alcohol was purchased from Fisher Scientific.

2.2. MWNT surface oxidization

In order to obtain a good dispersion of MWNT in PMMA, MWNTs were first treated with concentrated nitric acid to get rid of amorphous carbon on the tube walls and to introduce carboxyl groups. In a typical experiment, 100 mg of MWNTs was dispersed in 200 mL of concentrated nitric acid. The mixture was heated to maintain boiling in a refluxing system for 2 h. Then the oxidized MWNTs were washed by dispersing in water and filtering with poly (tetrafluoro ethylene) membranes multiple times. Finally, the oxidized MWNTs were dispersed in water and freeze dried.

2.3. Preparation of MWNT/PMMA nanocomposites

A solution-mixing method was chosen to prepare the MWNT/PMMA nanocomposites because it leads to good dispersion of MWNT and does not cause significant damage to the MWNT. In a typical experiment, 5 mg of oxidized MWNT was dispersed in anhydrous THF by water bath sonication for 6 min, followed by ultrasonication with a wand sonicator for 10 s, and then mixing with a THF solution of 1 g of PMMA by ultrasonicating for 30 s. The mixture was poured into a large quantity of ethanol stirred by a magnetic bar to facilitate precipitation of the composite. The precipitates were filtered out with a PTFE membrane and dried in vacuum oven at 70 °C. The dried nanocomposites were compounded with a hot press at 225 °C under two tons of load and were cooled down to room temperature under two tons of load. Two types of composites were prepared by this method: one with oxidized carbon nanotubes grown for 100 min (*M100*), the other with oxidized carbon nanotubes grown for 20 min (*M20*).

Transmission electron microscopy (TEM) was used to investigate the dispersion of MWNT in PMMA. The samples were microtomed at room temperature with a diamond knife at a thickness of 70 nm and mounted on a 200-mesh copper grid. Images were obtained with a Phillips CM12 using an accelerating voltage of 120 kV.

2.4. MWNT aspect ratio

In order to determine the aspect ratio of the MWNT after mixing with PMMA, 0.2 g of both nanocomposites (containing MWNTs grown for 20 or 100 min) were dissolved in 50 mL of THF at room temperature for 48 h. Each mixture was dropped on to a TEM copper grid covered with carbon film with a tissue paper underneath. While the PMMA/THF solution went through the carbon film and was absorbed by the tissue paper, most of the MWNTs were

retained on the carbon film. Field-emission scanning electron microscope (FESEM) images of MWNTs on the carbon films were taken and the lengths (L) of 150 nanotubes from each composite were measured to obtain statistically sound values. The aspect ratio was calculated by dividing L by the average diameter of 30 nm Fig. 2 shows a comparison of the aspect ratio of MWNT as obtained from FESEM analysis. Strong oxidizing groups of nitric acid can attack defective sites on carbon nanotubes [14] and strong shear force caused by sonication will damage carbon nanotubes, so both effects will shorten carbon nanotubes [15]. Average lengths of 11.26 ± 6.56 and 3.94 ± 2.73 μm were obtained for nantubes grown for 100 and 20 min, respectively. These lengths translate to an average aspect ratio of 377 and 130, respectively.

2.5. Foaming with supercritical carbon dioxide

To investigate the influence of MWNT aspect ratio on the bubble nucleation inside composites, a batch foaming process was used to make MWNT/PMMA nanocomposite foams. An autoclave (fixed head 4596 Micro Reactor with 4843 controller, Parr Instrument Co.) with a cylindrical chamber diameter of 2.54 cm, height of 5.08 cm, and volume of 25 mL was used. The stainless steel autoclave was rated for use up to 20.7 MPa at 350 °C. In a typical experiment, the composites were soaked in supercritical CO_2 at 40 °C and constant pressure for 24 h, and then the pressure was released quickly to induce bubble nucleation and initial growth. After foaming, the composites were taken out of the autoclave and immersed in room temperature water to vitrify the sample so that further bubble growth was restricted (*Foam I*). Both the pure PMMA and the nanocomposites were foamed at five different soaking pressures: 11.6, 12.7, 13.7, 15.8, and 17.9 MPa.

To investigate the influence of MWNT aspect ratio on the bubble density of nanocomposite foams after full bubble growth, some nanocomposites were foamed in boiling water after the supercritical CO_2 pressure was released. The water foaming was done by immersing the composites in 65 °C water for 5 min. Afterwards, the composites were taken out and immersed in room temperature water for 5 min (*Foam II*).

FESEM was used for bubble density analysis. Samples were freeze fractured in liquid nitrogen and the fracture surface was sputter-coated with gold. Typically, a micrograph showing more than 100 bubbles was chosen. Bubble density and bubble size analysis was conduced using ImageJ (National Institute of Health).

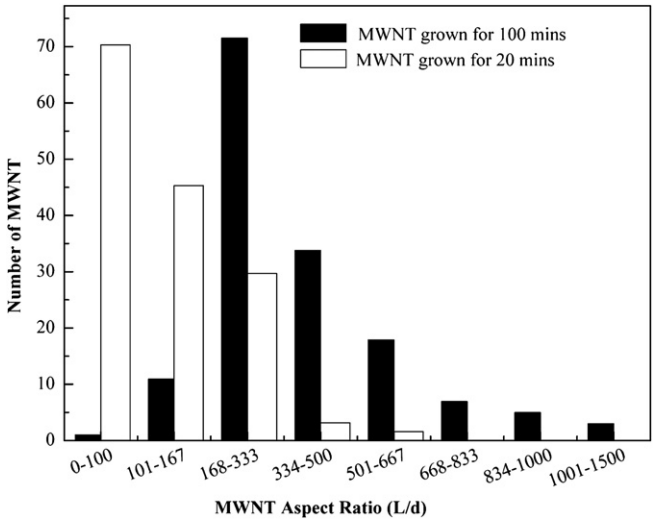

Fig. 2. A comparison of the aspect ratios of MWNTs grown for 100 and 20 min.

The number of bubbles (n) was counted from a collection of images at the same magnification (M). The number of bubbles per unit volume (ρ) was calculated using the following equation [16]:

$$\rho = \left(\frac{n \cdot M^2}{A}\right)^{3/2} \quad (1)$$

where A is the area of the SEM image.

3. Results and discussion

3.1. Dispersion of MWNTs in PMMA

Typical TEM images of the nanocomposites are shown in Fig. 3. The images indicate good dispersion of both types of MWNT in PMMA. No agglomerates were observed.

3.2. Foaming with supercritical carbon dioxide (Foam I)

A basic foaming process can be divided into three steps: (1) Mixing: formation of a homogeneous solution composed of a foaming agent and polymer matrix; (2) Bubble nucleation: phase separation induced by a thermodynamic instability usually due to a change in temperature or pressure; (3) Bubble growth and coalescence. All stages play crucial roles in determining the final foam morphology. However, in the first part of the current study, the nanocomposites were taken out of the autoclave quickly after the pressure was released, and were cooled to room temperature in water. As a result, step (3) was inhibited by the low mobility of polymer chains at room temperature (the glass transition temperature of PMMA is above 100 °C). It is expected that the foam morphology is mainly controlled by bubble nucleation and initial bubble growth inside the autoclave.

The bubble density of *Foam I* samples was investigated using FESEM. Fig. 4 shows the FESEM images of neat PMMA and the nanocomposites after foaming at saturation pressures of 15.8 and 17.9 MPa with supercritical carbon dioxide. The bubble density of all composite foams was calculated according to Equation (1). Fig. 5 shows the results.

There are several important points to note. First, the bubble density of the neat PMMA foam is smaller than the bubble density of the MWNT/PMMA nanocomposite foams. This result is expected because in the neat polymer the nucleation mechanism is homogeneous, whereas in the nanocomposites it is heterogeneous. Second, the bubble density increases with increasing saturation pressure. This can be explained by a decrease in bubble nucleation barrier with increasing saturation pressure [17]. Third, the

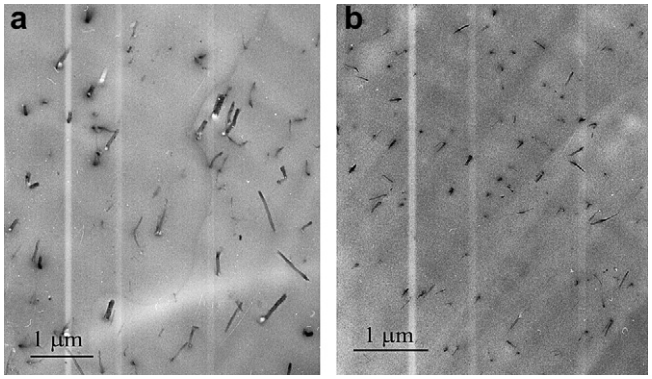

Fig. 3. TEM images of nanocomposites: *M100* (left) and *M20* (right).

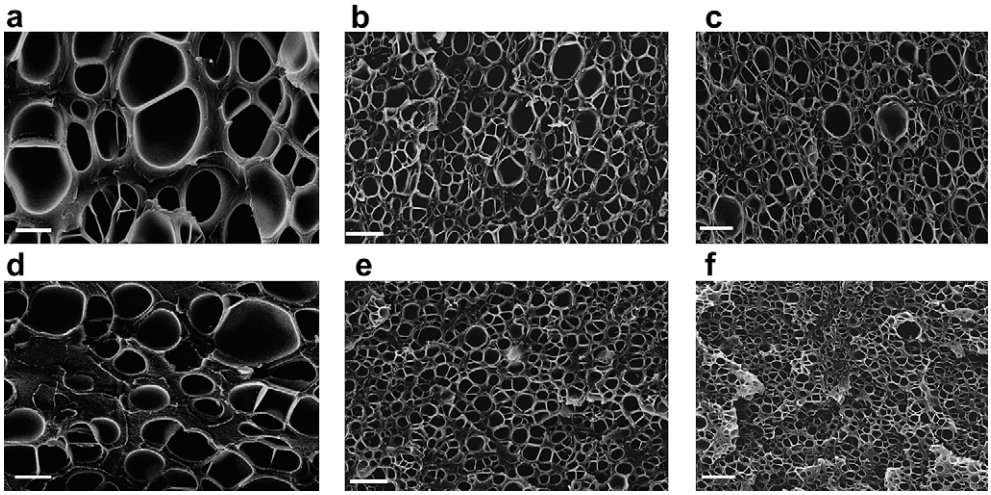

Fig. 4. FESEM micrographs of (a) neat PMMA, (b) *M100* nanocomposites, and (c) *M20* nanocomposites foamed at 17.9 MPa (top row); and (d) neat PMMA, (e) *M100* nanocomposites, and (f) *M20* nanocomposites foamed at 15.8 MPa (bottom row). Scale bar = 4 μm.

composites containing shorter MWNT (*M20*) yielded higher bubble density than the composites containing longer MWNT (*M100*).

The bubble nucleation process is commonly described by classical nucleation theory. In the case of polymer nanocomposite foams, heterogeneous nucleation theory is more suitable because the dispersed nanofillers provide a surface (or interface) to nucleate on, and lower the critical free energy of nucleation. In classical nucleation theory, the steady state, homogeneous nucleation rate is given as [18,19]:

$$N_o = n_o C_o \nu_o \cdot \exp\left(-\frac{\Delta G^*}{k_B T}\right) \tag{2}$$

where ΔG^* denotes the critical free energy of nucleation, k_B is the Boltzmann constant, T the absolute temperature, n_o is the concentration of heterogeneous nucleation sites, C_0 is the number of gas molecules dissolved per unit volume of polymer, and ν_o is the frequency factor of gas molecules merging with the nuclei and is believed to be weakly dependent on temperature [17].

For heterogeneous bubble nucleation, the critical free energy of nucleation (ΔG_{het}^*) is defined as follows:

$$\Delta G_{het}^* = \Delta G^* \frac{f(m,w)}{2} = \frac{16\pi\sigma^3}{3\Delta P^2}\frac{f(m,w)}{2} \tag{3}$$

where σ is the surface energy of the matrix, and ΔP is the pressure difference between the pressure of the metastable gas phase inside a nucleated bubble and the pressure of the gas phase outside the bubble upon nucleation. If the polymer is fully saturated with CO_2 and the partial molar volume of CO_2 in the polymer is zero, ΔP can be taken as the pressure drop required to induce nucleation, $P_{initial} - P_{final}$. The energy reduction factor, f, is a function of the contact angle (θ) and the relative curvature (w) of the nucleant surface ($w = R/r^*$ where R is the filler radius and r^* is the critical radius of the nucleus, $r^* = 2\sigma/\Delta P$). Fletcher defined the energy reduction factor for nucleation over a spherical surface as follows [18]:

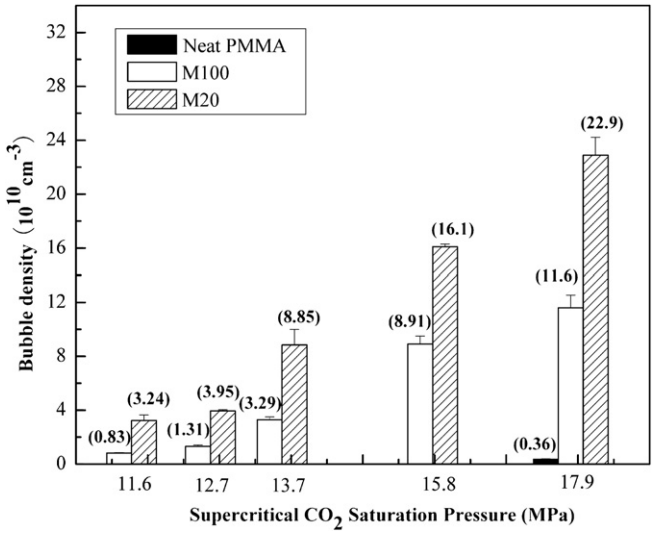

Fig. 5. A comparison of the bubble density of neat PMMA, *M100*, and *M20* nanocomposites foamed at various pressures. Error bars represent the standard deviations of bubble density data of four samples under each condition.

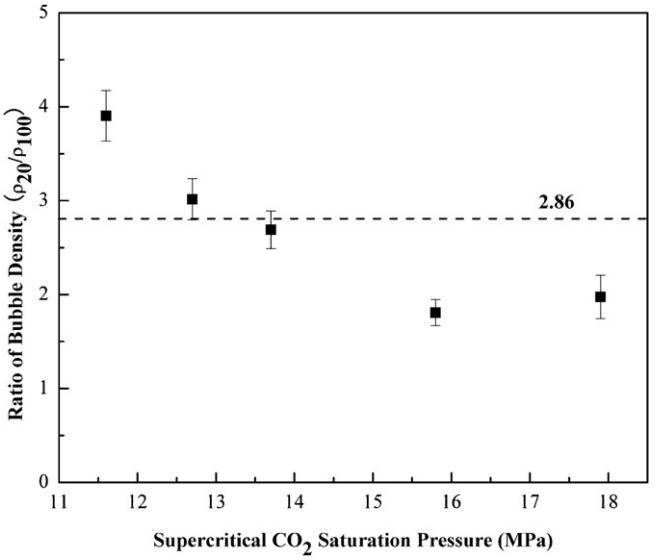

Fig. 6. The bubble density ratio of *M20* and *M100* nanocomposites. Error bars represent the standard deviations of bubble density ratios calculated based on the data shown in Fig. 7.

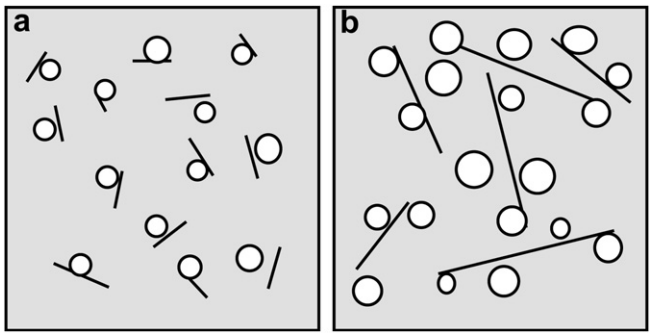

Fig. 7. A schematic indicating the possible nucleation behavior around carbon nanotubes: (a) each carbon nanotube acts as one nucleation site; (b) each carbon nanotube provides multiple nucleation sites.

$$f(m,w) = 1 + \left(\frac{1-mw}{g}\right)^3 + 3mw^2\left(\frac{w-m}{g} - 1\right) + w^3\left[2 - 3\left(\frac{w-m}{g}\right) + \left(\frac{w-m}{g}\right)^3\right], \quad (4)$$

where

$$m = \cos\theta$$
$$g = \left(1 + w^2 - 2mw^2\right)^{1/2} \quad (5)$$

Because the energy reduction factor depends on the contact angle [19,20] and relative curvature [18,19], ΔG_{het}^* also depends on both of these factors (see Eq. (3)).

The smaller the value of f, the larger the nucleation rate. The energy reduction factor decreases with decreasing contact angle at high relative curvatures. Therefore, small fillers and high contact angles result in a decreased nucleation rate.

In the current study, the curvature of the two fillers (*M100* and *M20*) used is the same. There are, however, two types of sites where bubbles can nucleate: at the ends or the sidewalls of the MWNT. The sidewalls are curved graphite structures that can be considered heterogeneous nucleation sites described by classical bubble nucleation theory. The ends of the MWNT, however, have so-called nanoscale cylindrical pore structure [21], which may trap CO_2 forming gas cavities [22–24]. Preexisting gas cavities can lower the critical free energy of nucleation drastically and facilitate rapid bubble nucleation [25]. In addition, it is known that chemical vapor deposition produces MWNTs ends with high defect concentration [26], Therefore, after nitric acid treatment, there may be more carboxyl groups at the ends of the MWNTs compared to the sidewalls [14]. It is known that the carboxyl group has high CO_2 affinity [27], thus the wettability of CO_2 on the carbon nanotube ends is higher than the wettability of CO_2 on the sidewalls. Such high CO_2 wettability leads to a smaller contact angle between CO_2 and the MWNT ends. According to Eq. (3), the ends of the MWNTs would have a lower energy barrier for heterogeneous nucleation. Therefore, it is reasonable to hypothesize that the MWNT ends are more effective heterogeneous nucleation sites compared to the sidewalls.

The concentration of MWNTs in all samples was kept constant. Therefore, the ratio of the number of MWNTs grown for 20 min to MWNTs grown for 100 min is indirectly proportional to their average lengths (the diameters of both MWNT were approximately the same) and is given as follows[1]:

$$\frac{n_{20}}{n_{100}} = \frac{L_{100}}{L_{20}} = \frac{11.26}{3.94} = 2.86 \quad (6)$$

[1] A more careful analysis using the distribution of lengths yielded the same ratio.

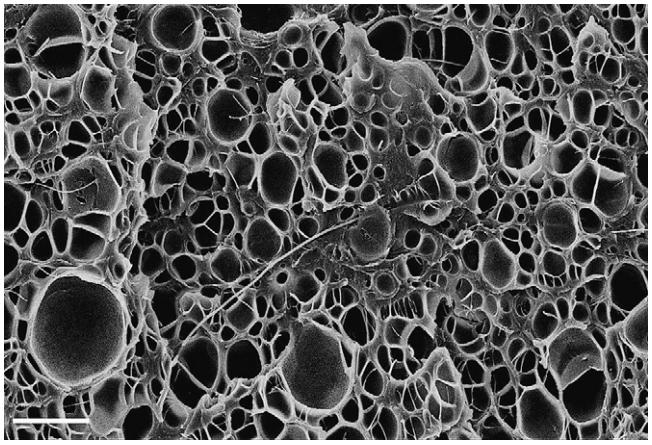

Fig. 8. *M100* nanocomposite foam showing that the nanotubes are longer than the distance between bubble nucleation sites. Scale bar = 4 μm.

If heterogeneous nucleation is the dominant mechanism and each nucleant acts as a single bubble nucleation site, then the bubble density (ρ) should be proportional to the number of MWNTs present in the system according to Eq. (3).

$$\frac{\rho_{20}}{\rho_{100}} = \frac{n_{20}}{n_{100}} = 2.86 \quad (7)$$

However, Fig. 6 shows that the bubble density ratio (ρ_{20}/ρ_{100}) decreases with increasing CO_2 saturation pressure and stabilizes around two. Therefore, additional factors must be affecting the bubble density.

Most heterogeneous nucleation models are based on the assumption that nucleants are spherically shaped and only one bubble nucleates on a given nucleant (or none at all) [28]. However, as the aspect ratio increases, the nanotube may shift from nucleating one bubble to multiple bubbles (compare Fig. 7a and b). Therefore, the number of possible heterogeneous nucleation sites is probably higher than the number of carbon nanotubes because of the potential for sidewall nucleation. The possibility of this happening should be higher for longer nanotubes. This phenomenon suggests that in the case of the nanocomposites filled with MWNTs grown for 100 min, there might be more than one nucleation event taking place along a given nanotube. Fig. 8 is presented in support of this claim. It shows a nanotube grown

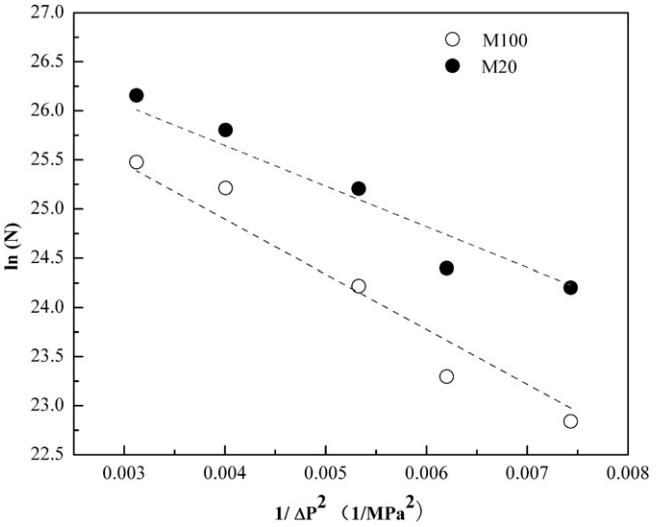

Fig. 9. Bubble density as a function of CO_2 saturation pressure. Dashed lines are linear least squares fit to data.

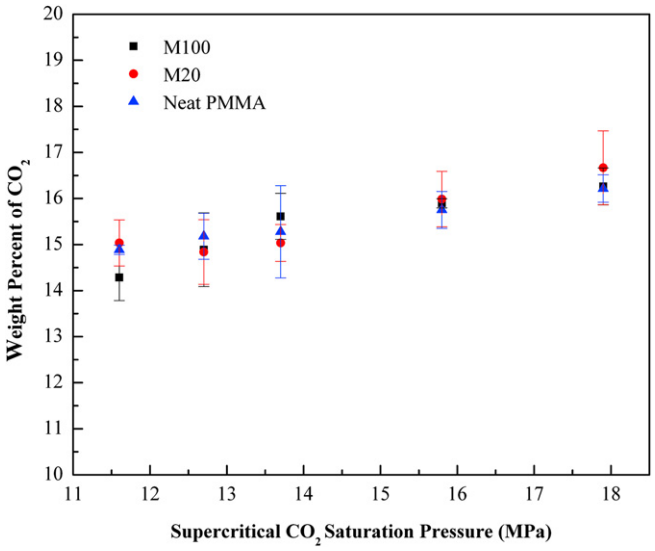

Fig. 10. Weight percent of CO_2 inside the composites or neat PMMA after the samples were soaked with supercritical CO_2 at 40 °C and then taken out of the pressure chamber following pressure release. Error bars represent the standard deviations of CO_2 weight percentage data for three samples under each condition.

for 100 min surrounded by multiple bubbles. The sidewall nucleation might explain the lower ratio of bubble density (ρ_{20}/ρ_{100}) than the ratio of the number of carbon nanotubes (n_{20}/n_{100}) as shown in Fig. 6.

If bubble nucleation in MWNT/PMMA nanocomposites follows the behavior shown in Fig. 7b, then the decrease in ρ_{20}/ρ_{100} with CO_2 saturation pressure might be the result of differences in ΔG_{het}^*. As mentioned earlier, there might be gas cavities trapped at the ends of the MWNT, and there should be more carboxyl groups on the nanotube ends after acid treatment, both of which would decrease the critical free energy for heterogeneous nucleation at the ends of the nanotubes. According to Eq. (3), the greater the ΔG_{het}^*, the faster the bubble nucleation rate decreases with decreasing supersaturation (ΔP). Therefore, if ΔG_{het}^* at the sidewall is greater than ΔG_{het}^* at the ends of the MWNT, then higher aspect ratio nanotubes (with more sidewall) will exhibit a faster decrease in nucleation rate with decreasing pressure, than shorter aspect ratio tubes. This is observed in Fig. 9. This leads to the increasing bubble density ratio (ρ_{20}/ρ_{100}) with decreasing pressure as shown in Fig. 6.

Homogeneous nucleation also occurs during any foaming operation [28], and it is not affected by the number of nucleation sites but strongly depends on the CO_2 saturation pressure according to Eq. (4). However, homogeneous nucleation becomes significant only at very high supersaturation conditions [29]. Fig. 5 shows that the bubble density in neat PMMA, which is a result of homogeneous nucleation, is much smaller than that observed in the nanocomposite foams. Therefore, the influence of homogeneous nucleation on the bubble density in the case of these nanocomposite foams is negligible.

3.3. Foaming with 65 °C water after $scCO_2$ soaking (Foam II)

As mentioned in the previous section, a basic foaming process includes three steps: mixing, bubble nucleation and bubble growth. In the first part of this research, the bubble growth process was intentionally inhibited by quickly vitrifying the polymer composites so that the bubble density in the composites reflected the bubble nucleation behavior without the influence of bubble coalescence. However, there was still a large quantity of CO_2 inside the polymer matrix after the composites were taken out from the pressure chamber. The remaining CO_2 could not expand the existing bubbles since the matrix was hardened at room temperature. Fig. 10 shows the weight percent of CO_2 remaining inside the composites and neat PMMA after the samples were soaked with supercritical CO_2 at 40 °C at several saturation pressures and then taken out of the pressure chamber following sudden pressure release. The data was obtained by weighing the samples both before the supercritical CO_2 soaking process and right after the pressure release. The weight difference is the weight of CO_2 trapped inside the samples. It was found that there was more than 14 wt% of CO_2 inside the PMMA after the samples were taken out of the chamber. The relative amount of trapped CO_2 by weight decreased with decreasing soaking pressure. The reason for this is that although the samples were at room temperature and under atmospheric pressure when taken out of the chamber, the supersaturated CO_2 inside the sample could not diffuse fast enough to reach equilibrium right away. It was also found that the amount of CO_2 trapped inside the composites and neat PMMA was similar, which indicates that the MWNT inside the composites and the aspect ratio of MWNT did not affect the solubility of CO_2 in the composites significantly. This finding agrees with the finding of Taki and coworkers [30], who found that the solubility of CO_2 in

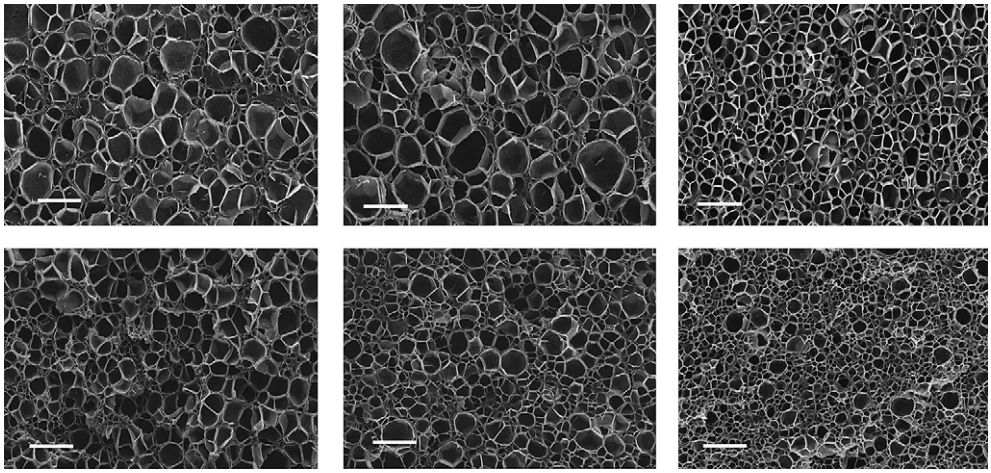

Fig. 11. FESEM micrographs of *M100* (top row) and *M20* (bottom row) nanocomposites foamed at 11.6 MPa (left column), 13.7 MPa (middle column) and 17.9 MPa (right column) with subsequent 65 °C water immersion (*Foam II*). Scale bar = 10 μm.

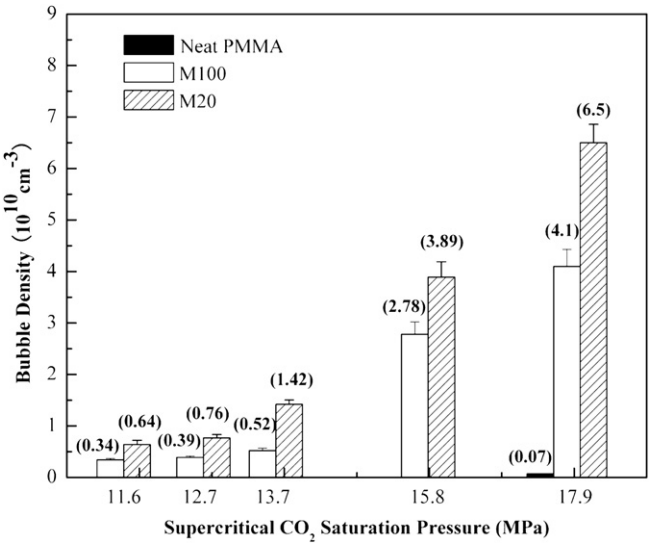

Fig. 12. A comparison of the bubble density of neat PMMA, *M100*, and *M20* nanocomposites foamed at various pressures with subsequent 65 °C water immersion (*Foam II*). Error bars represent the standard deviations of the bubble density data for three samples under each condition.

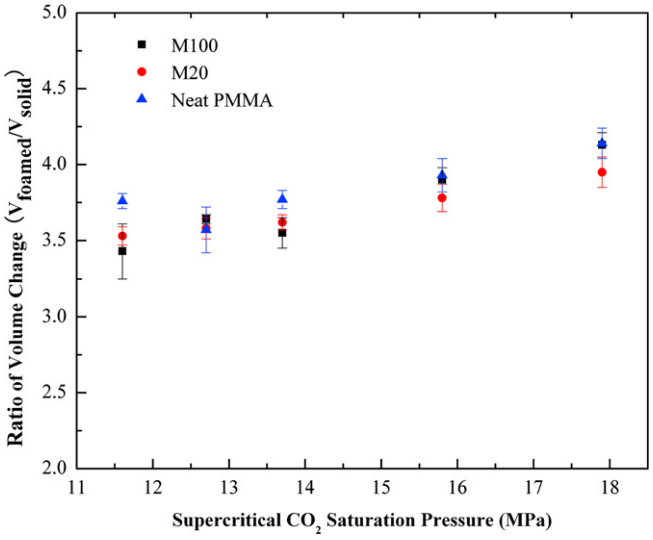

Fig. 13. The ratio of the volume change before and after the supercritical CO_2 foaming process with hot water immersion (*Foam II*). Error bars represent the standard deviations for three samples under each condition.

nanoclay/polypropylene composites did not change with filler content. To utilize the remaining CO_2 to generate foamed structures and lighter materials, the composites were put into 65 °C water for 5 min.

Fig. 11 shows the FESEM images of the nanocomposites after foaming at saturation pressures of 11.6, 13.7 and 17.9 MPa with supercritical carbon dioxide and 5 min immersion in 65 °C water. The bubble density of all composite foams was calculated according to Eq. (1) (see Fig. 12).

Fig. 12 shows the same trend as Fig. 5. The bubble density of the neat PMMA foam is smaller than that of the nanocomposite foams, and the bubble density increases with increasing saturation pressure and decreasing MWNT aspect ratio. This is because bubble nucleation plays a significant role in determining the final foam structure. The decrease in bubble density resulted in the creation of larger bubbles as seen from Fig. 11 and Table 1.

When the samples, supersaturated with CO_2 at room temperature under atmosphere pressure, were immersed into 65 °C water, multiple processes occurred. First, the polymer softened due to increased temperature. Second, at constant pressure, the solubility of CO_2 inside PMMA decreased with increasing temperature [31,32]. As a result the supersaturation of CO_2 inside the composites increased after the composites were immersed into hot water. Third, the supersaturated CO_2 phase separated from the matrix, and the phase separated CO_2 diffused into the existing bubbles to promote bubble growth, diffused out of the samples, or induced new bubble nucleation and growth. Finally, if the bubbles grow, bubble coalescence can occur [30]. In the current study, the reduced bubble density after water immersion indicates that there was bubble coalescence during the process. The weight of the foams is similar to the weight of the solid composites after the water immersion process, indicating that a lot of carbon dioxide escaped out of the matrix by diffusion. However, the remaining CO_2 did expand, increasing the sample volume. Fig. 13 shows that the sample volume increased by a factor of 3.5–4.0.

Table 1
Average bubble radius of *M100* and *M20* nanocomposites foamed under various conditions.

Pressure[a] (MPa)	Average bubble radius (μm)			
	Foam I		*Foam II*	
	M100	*M20*	*M100*	*M20*
17.9	0.76	0.44	1.39	0.91
15.8	0.82	0.62	1.83	1.28
13.7	0.96	0.67	2.50	1.49
12.7	1.02	0.76	2.51	1.78
11.6	1.06	0.78	2.56	1.94

[a] Supercritical CO_2 saturation pressure.

4. Conclusions

Poly(methyl methacrylate), PMMA, and multi walled carbon nanotube (MWNT)/PMMA nanocomposites containing MWNT with two different average aspect ratios (377 and 133) were foamed using supercritical carbon dioxide at various saturation pressures with or without subsequent hot water immersion. The MWNT aspect ratio distribution and dispersion in PMMA matrix was investigated with field-emission scanning electron microscopy (FESEM) and transmission electron microscopy (TEM). Bubble density was obtained from FESEM images. It was found that at the same MWNT concentration (by weight), nanocomposites filled with higher aspect ratio MWNTs have a lower bubble volume density than those filled with lower aspect ratio MWNTs when foamed at the same condition. Bubble density was found to depend on saturation pressure. At low saturation pressures, it is believed that nucleation occurs mainly at the nanotube ends, because the critical free energy of nucleation is lower at the nanotube ends than the sidewalls; hence, nanocomposites with shorter nanotubes show greater bubble density. On the other hand, at high saturation pressures, nucleation at the nanotube sidewalls becomes feasible and longer nanotubes act as multiple nucleation sites leading to an increased bubble density in the higher aspect ratio MWNT nanocomposites.

Acknowledgements

Financial support from the Nanoscale Science and Engineering Initiative of the National Science Foundation under NSF Award Number DMR-0117792 and CMMI-0500324 is gratefully acknowledged.

References

[1] Li Y, Chen C, Zhong S, Ni Y, Huang J. Electrical conductivity and electromagnetic interference shielding characteristics of multiwalled carbon nanotube filled polyacrylate composite films. Appl Surf Sci 2008;254:5766–71.

[2] Yang YL, Gupta MC, Dudley KL, Lawrence RW. A comparative study of EMI shielding properties of carbon nanofiber and multi-walled carbon nanotube filled polymer composites. J Nanoscience Nanotechnol 2005;5:927–31.
[3] Lu G, Li X, Jiang H. Electrical and shielding properties of ABS resin filled with nickel-coated carbon fibers. Compos Sci Technol 1996;56:193–200.
[4] Chung DDL. Electromagnetic interference shielding effectiveness of carbon materials. Carbon 2000;39:279–85.
[5] Chung DDL. Materials for electromagnetic interference shielding. J Mater Eng Perform 2000;9:350–4.
[6] Thomassin J-M, Pagnoulle C, Bednarz L, Huynen I, Jerome R, Detrembleur C. Foams of polycaprolactone/MWNT nanocomposites for efficient EMI reduction. J Mater Chem 2008;18:792–6.
[7] Li N, Huang Y, Du F, He X, Lin X, Gao H, et al. Electromagnetic interference (EMI) shielding of single-walled carbon nanotube epoxy composites. Nano Lett 2006;6:1141–5.
[8] Bauhofer W, Kovacs JZ. A review and analysis of electrical percolation in carbon nanotube polymer composites. Compos Sci Technol 2009;69:1486–98.
[9] Monirruzzaman M, Winey KI. Polymer nanocomposites containing carbon nanotubes. Macromolecules 2006;39:5194–205.
[10] Zeng C, Hossieny N, Zhang C, Wang B. Synthesis and processing of PMMA carbon nanotube nanomposite foams. Polymer 2010;51:655–64.
[11] Lee LJ, Zeng C, Cao X, Han X, Shen J, Xu G. Polymer nanocomposite foams. Compos Sci Technol 2005;65:2344–63.
[12] Bult J. Controlled carbon nanotube synthesis for quantification of polymer-nanotube composite micromechanics. PhD Dissertation, Rensselaer Polytechnic Institute; 2007. p. 19–21.
[13] Gross S, Camozzo D, Noto VD, Armelao L, Tondello E. PMMA: a key macromolecular component for dielectric low-κ hybrid inorganic–organic polymer films. Eur Polym J 2007;43:673–96.
[14] Zhang J, Zou H, Qing Q, Yang Y, Li Q, Liu Z, et al. Effect of chemical oxidation on the structure of single-walled carbon nanotubes. J Phys Chem B 2003;107:3712–8.
[15] Hennrich F, Krupke P, Arnold R, Stutz JAR, Lebedelkin S, Koch T, et al. The mechanism of cavitation-induced scission of single-walled carbon nanotubes. J Phys Chem 2007;111:1932–7.
[16] Kumar V, Suh NP. A process for making microcellular thermoplastic parts. Polym Eng Sci 1990;30:1323–9.
[17] Goren K, Chen L, Schadler LS, Ozisik R. Influence of nanoparticle surface chemistry and size on supercritical carbon dioxide processed nanocomposite foam morphology. J Supercrit Fluids 2010;51:420–7.
[18] Fletcher NH. Size effect in heterogeneous nucleation. J Chem Phys 1958;29:572–6.
[19] Shen J, Zeng C, Lee LJ. Synthesis of polystyrene-nanofibers nanocomposite foams. Polymer 2005;46:5218–24.
[20] Zeng C, Han X, Lee LJ, Koelling KW, Tamosko DL. Polymer-clay nanocomposite foams prepared using carbon dioxide. Adv Mater 2003;15:1743–7.
[21] Aleksey V, Alexander N. Nucleation of liquid bridges and bubbles in nanoscale capillaries. J Chem Phys 2003;119:9755–64.
[22] Yang Q, Hou P, Bai S, Wang M, Cheng H. Adsorption and capillarity of nitrogen in aggregated multi-walled carbon nanotubes. Chem Phys Lett 2001;345:18–24.
[23] Rende D, Baysal N, Ozisik R. Carbon dioxide sequestration by carbon nanotubes: application of graph theoretical approach. Computational Materials Science 2010;48:402–8.
[24] Rende O, Ozgur L, Baysal N, Ozisik R. Carbon dioxide sequestration by single walled carbon nanotubes; in preparation.
[25] Jones SF, Evans GM, Galvin KP. Bubble nucleation from gas cavities- a review. Adv Colloid Interface Sci 1999;80:27–50.
[26] Louie SG. Electrical properties, junctions and defects of carbon nanoutbes. Top Appl Phys 2001;80:113–45.
[27] Shieh Y, Liu K. The effect of carbonyl groups on gas sorption of CO_2 in glass polymers. J Supercrit Fluids 2003;25:261–8.
[28] Lee LJ, Zeng C, Cao X, Han X, Shen J, Xu G. Polymer nanocomposite foams. Compos Sci Technol 2005;65:2344–63.
[29] Liu XY. Effect of foreign particles: a comprehensive understanding of 3D heterogeneous nucleation. J Cryst Growth 2002;237–239:1806–21.
[30] Taki K, Tababa K, Kihara S, Oshima M. Bubble coalescence in foaming process of polymers. Polym Eng Sci 2006;46:680–90.
[31] Goel SK, Beckman EJ. Plasticization of poly(methyl methacrylate) PMMA networks by supercritical carbon dioxide. Polymer 1993;34:1410–7.
[32] Goel SK, Beckman EJ. Generation of microcellular polymeric foams using supercritical carbon dioxide. I: effect of pressure and temperature on nucleation. Polym Eng Sci 1994;34:1137–47.